Electronic Supplementary Material (ESI) for Journal of Materials Chemistry C.

High Hole Mobilities in Two Dimensional Monolayer MSi_2Z_4 (M = Mo/W; Z = P, As, Sb) for Solar Cells

Xia Qiu[a,d], Wangping Xu*[b,d], Weixiang Kong[a,d], Xiaoliang Xiao[a,d], Rui Wang[a,d], Jing Fan[c], and Xiaozhi Wu*[a,d]

a: Institute for Structure and Function and Department of Physics, Chongqing University, Chongqing 401331, P. R. China
b: Hunan Institute of Advanced Sensing and Information Technology, Xiangtan University, Xiangtan 411105, P. R. China
c: Center for Computational Science and Engineering, Southern University of S cience and Technology, Shenzhen 518055, P. R. China
d: Chongqing Key Laboratory for Strongly Coupled Physics, Chongqing Univer sity, Chongqing 401331, P. R. China

Recently, centimeter-scale monolayer $MoSi_2N_4$ (α_1-phase) was successfully synthesized in experiments with excellent ambient stability. However, it is an indirect band gap semiconductor, which hinders its wide application. Here, we systematically studied the stability of structure and optoelectronic properties of both two new α_1-phase monolayers ($MoSi_2Sb_4$ and WSi_2Sb_4) and a new family α_2-phase monolayer MSi_2Z_4 (M = Mo, W; Z = P, As and Sb) by first-principles calculations. Our results indicated that all of these monolayer structures show high structural stability, and the α_2-phase structures are more stable than the α_1-phase structures. Moreover, all of them have direct band gaps with fascinating optical absorption efficiencies ranging from infrared to visible light. Importantly, the high hole mobility (up to 10^5 $cm^2V^{-1}s^{-1}$) reveals these monolayer MSi_2Z_4 will have potential applications in photoelectric devices. In addition, the α_2-$MoSi_2P_4$ possesses a desirable power conversion efficiency of 20.3%. Interestingly, spin-orbit coupling plays a key factor in exploring the optoelectronic properties of MSi_2Z_4 ternary compounds. These new ternary monolayer structures can effectively broaden the 2D materials family and provide promising potential candidates for optoelectronic applications.

*E-mail: xuwp@xtu.edu.cn

*E-mail: xiaozhiwu@cqu.edu.cn

Introduction

Two-dimensional (2D) optoelectronic materials have attracted a great amount of research attention in the past decade because of their tunable band structure, excellent electron transport properties, and large exciton binding energy.[1,2] It is well known that the outstanding 2D optoelectronic materials demand both reasonable direct band gap and ultrahigh carrier mobility.[3,4] Therefore, screening the innovative two-dimensional (2D) materials with fascinating mobility and desirable direct band gap is inspired not only by the interest in fundamental research but also by the actual need for applications of optoelectronic devices.

To date, the synthesized transition metal sulfides represented by MoS_2 have a sufficient band gap (1.7~2.5 eV) but unimpressive low carrier mobility (~10^2 $cm^2V^{-1}s^{-1}$).[5-7] Although black phosphorus (BP)[8] shows extremely high anisotropic carrier mobility and moderate band gap,[9,10] it is prone to oxidative degradation in the air, [11-13]which hinders its potential applications in electronic devices. Moreover, many other 2D layered optoelectronic materials have been experimentally synthesized, including layered group III-VI (InSe, GaSe)[14-16], group IV-V(*i.e.*, SnAs, GeAs, SiAs, GeP_3, and SnP_3)[17-20] and group VI-IV (*i.e.*, $PdSe_2$, GeS, and SnS)[21-23] binary compounds, the corresponding monolayer structures are shown desirable band gap and ultrahigh carrier mobility (up to ~10^4 $cm^2V^{-1}s^{-1}$). And the AsSb[24], BiAs[25], SiP[26], and BiSb[4] were also forecasted to possess tunable band gaps and high carrier mobilities. Recently, experimental evidence suggests that ultrathin (2.4 nm) $PbSnS_2$ sheets possess not only a large anisotropic photoresponse but also highly anisotropic hole mobility synthesized by the chemical vapor deposition (CVD) method.[27,28] Furthermore, synthesized layered SnP_2S_6 exhibits excellent photosensitive capabilities in addition to its rich piezoelectric properties and ionic conductivity.[29,30] It is investigated that the synthesized ternary compounds exhibit not only favorable performance in band gap and carrier mobility but also high stability, and their variable stoichiometric ratios provide the construction of abundant 2D optoelectronic materials.

Importantly, centimeter-scale monolayer $MoSi_2N_4$ (defined as α_1-phase) was successfully synthesized by the CVD method with excellent ambient stability.[31]

Following the success of monolayer $MoSi_2N_4$, more $MoSi_2N_4$-like (α_1-phase) optoelectronic materials have been predicted theoretically via high-throughput elemental substitution, which notably displays varied electronic properties including antiferromagnetic metals, semimetals, and semiconductors.[32-34] However, most of the semiconductors are indirect band gaps (i.e., $MoSi_2N_4$)[31], which significantly hinders their application.

Therefore, in this work, both the monolayer Mo/WSi_2Sb_4 (α_1-phase) and a new family of α_2-phase monolayer MSi_2Z_4 are proposed. We systematically studied the structural stability and optoelectronic properties using the first-principles calculations. Our results show that all of these monolayer structures show high structural stability and antioxidant ability, especially the α_2-phase structures are more stable than the α_1-phase structures. Moreover, all of them own direct band gaps with fascinating optical absorption efficiencies ranging from infrared to visible light. Furthermore, the high carrier mobility reveals these monolayer MSi_2Z_4 will have potential applications in photoelectric devices. Importantly, we have minutely discussed the effect of spin-orbit coupling (SOC) for optoelectronic properties on monolayer MSi_2Z_4. In addition, our proposed α_2-$MoSi_2P_4$ monolayer may have good applications as donor materials for solar cells.

Methods

All of the calculations are implemented by the Vienna Ab initio Simulation Package (VASP) which is based on density functional theory[35-37]. The generalized gradient approximation of the Perdew-Burke-Ernzerhof (PBE)[38-40] generalization is applied to describe the exchange-correlation generalization[41]. The cutoff energy and the k-points were set to be 500 eV and 16×16×1 for optimization structures, respectively. The convergence criteria for energy and force were set to be 10^{-6} eV and 0.01 eV/Å. Meanwhile, the vacuum space was set to be over 20 Å. The high-precision Heyd-Scuseria-Ernzerhof hybrid functional (HSE06)[42] was adopted to correct the band gap values due to the underestimated by the PBE. In addition, the van der Waals interactions (DFT-D3)[43] correction was used, and the climbing image nudged elastic band (CI-

NEB)[44] method was used to calculate the O_2 decomposition of barrier in monolayer α_2-$MoSi_2P_4$ surfaces.

Results and Discussion

Motivated by the monolayer $MoSi_2N_4$ synthesized in experiments, two new α_1-Mo/WSi_2Sb_4 and four α_2-MSi_2Z_4 monolayers (M = Mo, W; Z = P, As) are proposed in our work. The monolayer MSi_2Z_4 (M = Mo, W; Z = P, As, Sb) is hexagonal lattices and consists of seven atomic films, which can be considered composed of monolayer SiZ (Z = P, As, Sb) and monolayer MZ_2 (M = Mo/W, X = P, As, Sb) forming a sandwich-like intercalation structure. The difference between α_1-phase and α_2-phase monolayer MSi_2Z_4 is the location of top and bottom Z atoms, as shown in Fig. 1**.** The outermost two Z atoms and the W/Mo atoms are located at the same vertical line, as shown in Fig. 1(d). And the full optimization lattice constants of monolayer MSi_2Z_4 are listed in Table 1**.**

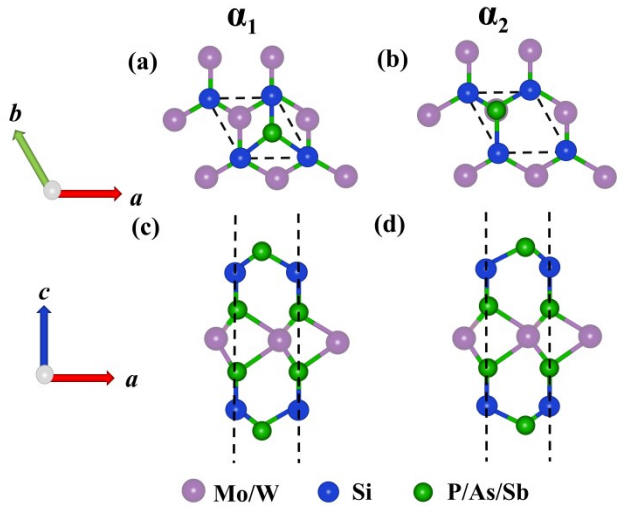

Fig. 1 Top and side views of MSi_2Z_4 (M = Mo, W; Z = P, As) monolayer with (a and c) α_1 and (b and d) α_2-phases. The hexagonal protocellular lattices are represented by Black dotted lines. The M, Si, and Z atoms are indicated by the purple, blue, and green balls, respectively.

To verify the structural stability of the optimized crystals MSi_2Z_4 (M = Mo, W; Z = P, As, Sb), we first estimated the cohesive energy of the crystals, the results are indicated in Table S1. The calculated cohesive energy of α_1-$MoSi_2P_4$ is -6.506 eV/atom, which is excellently consistent with the prior literature results[45]. The cohesive energy

of these monolayer MSi_2Z_4 is negative, and the lowest cohesive energy of α_2-$MoSi_2P_4$ is -6.786 eV/atom, significantly higher than that of molybdenum disulfide (-4.98 eV/atom)[46] and phosphorene (-3.30 eV/atom)[47] compounds. Interestingly, the cohesive energy of α_2-phase structures is lower than the α_1-phase monolayer MSi_2Z_4, revealing higher structural stability. Therefore, we mainly discuss the α_2-MSi_2Z_4 conformation in the following study. Furthermore, the vibrational phonon spectra and the ab initio molecular dynamics (AIMD)[48] simulations of these monolayer MSi_2Z_4 (M = Mo, W; Z = P, As) were systemically studied at 300 K, the results are shown in Fig. 2 and Fig. S1. Clearly, there are no imaginary frequencies found for these monolayer MSi_2Z_4 (see Fig. 2), and the total energy of structural snapshots of the *p* (4×4) supercell at 3 ps (see Fig. S1) are convergent, indicating that they are dynamically and thermodynamically stable.

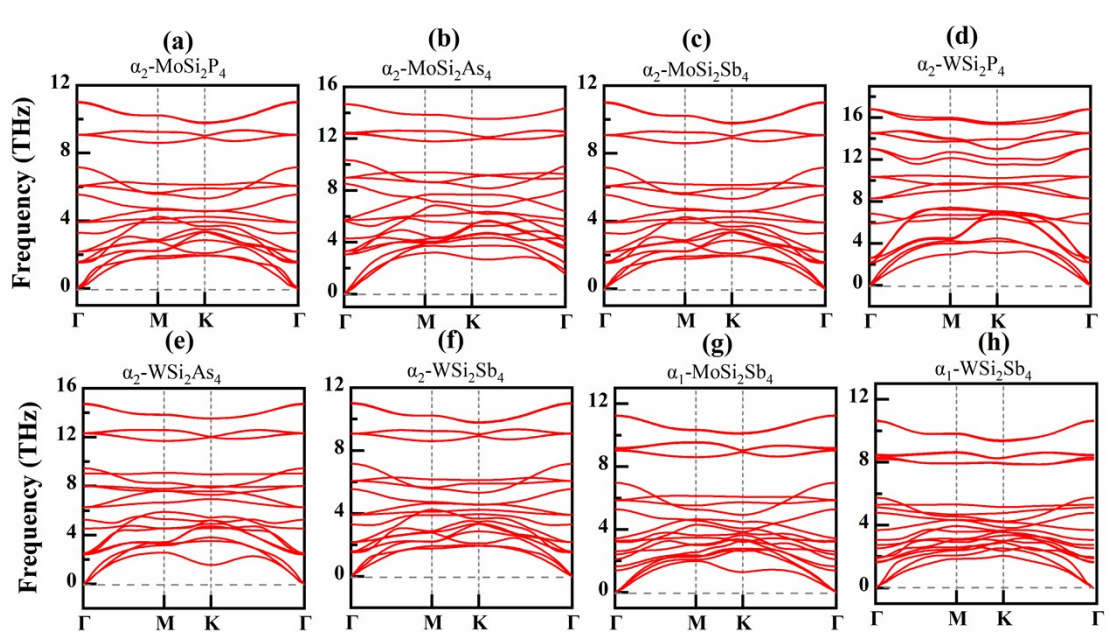

Fig. 2 Phonon spectra of eight monolayer (a)-(f) α_2-MSi_2Z_4 (A = Mo/W, Z = P, As, Sb), (g) α_1-$MoSi_2Sb_4$, and (h) α_1-WSi_2Sb_4 crystal structures.

As we know, the part of 2D optoelectronic materials is easily oxidized in ambient air (i.e., phosphorene, PAs, Ti_3C_2),[49-52] which hinders their wide application. Here, take the monolayer α_2-$MoSi_2P_4$ as an example, we considered the situation of O_2 adsorption decomposition on the *p*(4×4) α_2-$MoSi_2P_4$ surface, and the results are presented in Fig. S2. Our findings indicate that the O atoms tend to adsorb on top of the P atoms, and the

corresponding dissociation barrier is 1.08 eV, which is prominently larger than that on the black phosphorus surface (0.54 eV)[53], revealing a high antioxidant ability at room temperature.

Table 1 Structural and electronic properties of the 2D ML MSi_2Z_4 (M = Mo/W, Z = P, As, Sb) materials. Shown are the lattice parameters, a and b, the fundamental band gaps calculated with the HSE06, E_g^{HSE06}, and PBE functional, E_g^{PBE}. Direct bandgaps with SOC are considered in monolayer WSi_2Z_4 (Z= P, As, and Sb). Direct bandgaps with and without SOC are defined as D and D^{soc}.

Structure	Lattice constant a = b (Å)	E_g (eV)		Structure	Lattice constant a = b (Å)	E_g (eV)	
		E_g^{PBE}	E_g^{HSE06}			E_g^{PBE}	E_g^{HSE06}
α_1-$MoSi_2P_4$	3.47	0.68 (D)	0.97 (D)	α_2-$MoSi_2P_4$	3.46	0.91 (D)	1.20 (D)
α_1-$MoSi_4As_4$	3.62	0.60 (D)	0.84 (D)	α_2-$MoSi_4As_4$	3.61	0.76 (D)	1.02 (D)
α_1-$MoSi_2Sb_4$	3.90	0.38 (D)	0.63 (D)	α_2-$MoSi_2Sb_4$	3.89	0.51 (D)	0.77 (D)
α_1-WSi_2P_4	3.48	0.29 (D^{soc})	0.38 (D^{soc})	α_2-WSi_2P_4	3.46	0.61 (D^{soc})	0.77 (D^{soc})
α_1-WSi_2As_4	3.63	0.21 (D^{soc})	0.25 (D^{soc})	α_2-WSi_2As_4	3.61	0.44 (D^{soc})	0.51 (D^{soc})
α_1-WSi_2Sb_4	3.91	0.03 (D^{soc})	0.18 (D^{soc})	α_2-WSi_2Sb_4	3.90	0.13 (D^{soc})	0.07 (D^{soc})

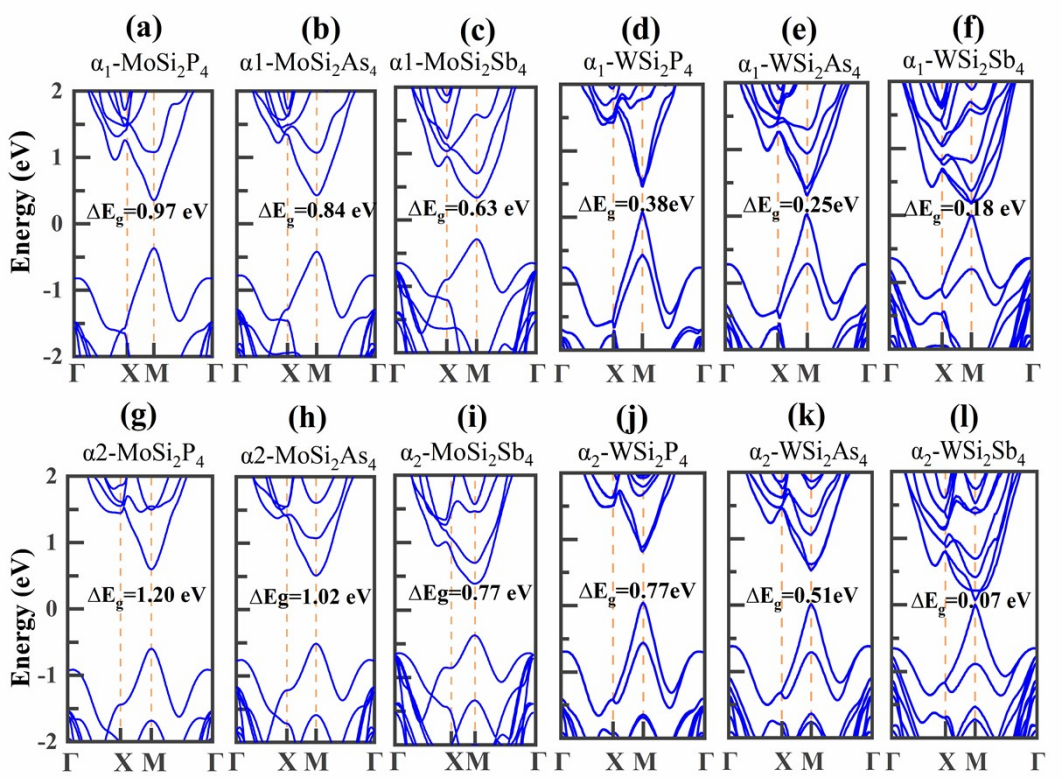

Fig. 3 The electronic band structure of all considered ML MSi_2Z_4 (M = Mo/W, Z=P, As, Sb) is calculated based on HSE06. Here, the Fermi level is set to zero. The band structures with SOC are considered in monolayer WSi_2Z_4 (Z= P, As, and Sb).

Since the electronic structure with the direct band gap is very superior to two-

dimensional photoelectric materials, we systemically computed the band structures of these our proposed monolayer MSi_2Z_4 (M = Mo, W; Z = P, As, Sb). However, the normal PBE grossly underrates the band gap. Take the α_2-$MoSi_2P_4$ for example, the band gaps obtained with PBE and HSE06 methods are 0.91 eV and 1.20 eV without SOC, respectively. It is found that the HSE06 band gap is beyond more than 30% compared with the PBE level. Thus, the high-precision HSE06 correction was adopted in the following calculations. As we know, the SOC effects may have a large influence on the optoelectronic properties of two-dimensional materials due to the heavy atoms of the compound. Therefore, the electronic structures with SOC effects have been considered for all monolayer MSi_2Z_4 by PBE level, as shown in Fig. S10. The results indicated that the SOC slightly change the band structures of monolayer $MoSi_2Z_4$. On the contrary, for monolayer WSi_2Z_4, the SOC can significantly reduce the band gaps with still direct band gaps. Thus, the SOC effects are considered to calculate electronic structure and light absorption spectra in monolayer WSi_2Z_4.

The band structures of these MSi_2Z_4 (M = Mo, W; Z = P, As, Sb) monolayers are illustrated in Fig. 3, and corresponding band gaps are listed in Table 1. All of these MSi_2Z_4 monolayers are direct band gap semiconductors, and the valence-band maximum (VBM) and conduction-band minimum (CBM) are located at the K points. It is worth noticing that the band cleavage is stronger in monolayer α_2-WSi_2Sb_4, which will lead to a smaller band gap calculated by HSE06 than that of by PBE level, as shown in Fig. S11. The values of the band gap are from 0.07 eV (α_2-WSi_2Sb_4) to 1.20 eV (α_2-$MoSi_2P_4$), which are located in the favorable range for infrared adsorption. Interestingly, the shape of the band structures is similar due to the small structural differences between the α_1-MSi_2Z_4 and α_2-MSi_2Z_4, but the band gaps are very different. For example, the band gap of α_1-$MoSi_2P_4$ is 0.97 eV, while the band gap of α_2-$MoSi_2P_4$ is 1.20 eV. It means the α_2-phase MSi_2Z_4 is more stable, which is in line with our previous conclusion.

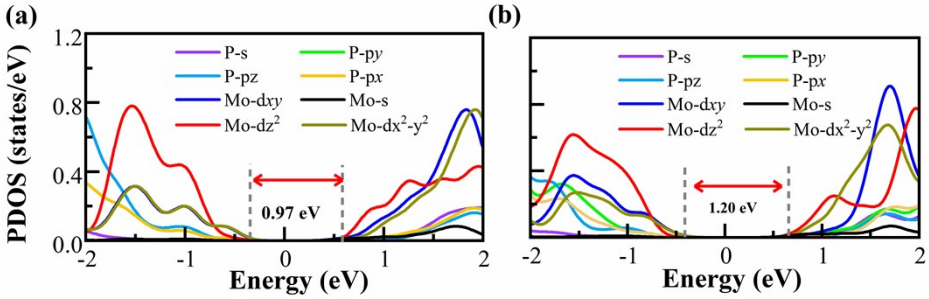

Fig. 4 The Projected State Density degree (PDOS) of (a) α_1-$MoSi_2P_4$ and (b) α_2-$MoSi_2P_4$ are calculated by the HSE06 functional.

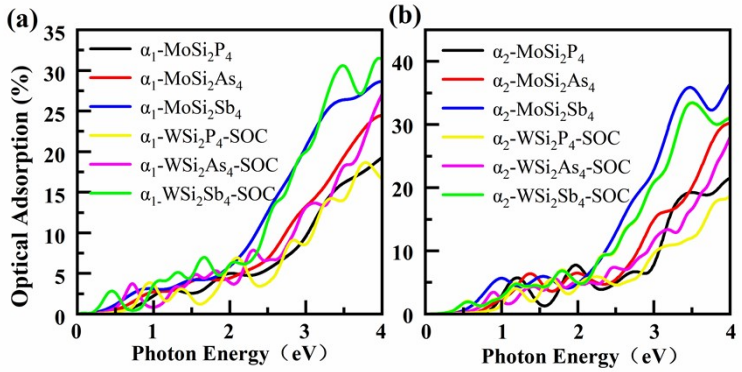

Fig. 5 The light absorption of monolayers (a) α_1-MSi_2Z_4 and (b) α_2-MSi_2Z_4 (M = Mo/W, Z = P, As, Sb) were calculated by HSE06 level. The light absorption of WSi_2Z_4 was calculated by considering the SOC effect.

Moreover, the orbital contribution of CBM and VBM has also been analyzed by both fat-band structures (see Fig. S3) and the density of states (see Fig. 4). Take the monolayer α_1/α_2-$MoSi_2P_4$ as an instance, the results indicate that the CBMs are mainly contributed by the dz^2, dx^2-y^2, and dxy orbital of Mo/W atoms, while the VBMs mainly originated from the d orbital of Mo/W atoms and slightly are dedicated originated from 2p orbitals of P atoms. Meanwhile, the optical absorption spectrums of both α_1- and α_2-phase MSi_2Z_4 monolayers were calculated with the HSE06 level. Our results reveal that these monolayer structures exhibit good light absorption ability from the infrared to visible light wavelengths, revealing they may have higher adsorption efficiency.

Carrier mobility is another significant factor in enhancing photoelectric materials' carrier transport ability. High carrier mobility means that the electrons and holes pair produced by adsorption photon can quickly participate in the response, corresponding to high photoelectric conversion efficiency.[54] Therefore, based on the deformation

potential (DP) method[55], we systematically investigated the carrier mobilities of both α_1- and α_2-phase MSi_2Z_4 at room temperature (300 K). Since the SOC can increase most curvature for VBM and CBM, especially for WSi_2Z_4, which will significantly reduce the effective mass. Therefore, all of the parameters of carrier mobilities have been calculated with and without SOC, as shown in Table 2. The detailed process calculated is listed in the supporting information, and the corresponding parameters are displayed in Table 2. The corresponding fitting of each parameter is shown in Fig. S4-S9. And the carrier mobility of x-direction and y-direction represent the zigzag direction and armchair direction, respectively. The results indicated that the SOC can slightly influence the deformation potential and elastic modulus. However, the SOC can significantly decrease the effective mass of monolayer MSi_2Z_4 in most cases. For example, the effective mass of α_2-WSi_2Sb_4 was reduced by more than 58%, which will result in the largest carrier mobility. The results indicated that most of the electrons and holes' mobilities are beyond 10^3 $cm^2V^{-1}s^{-1}$. More importantly, α_2-WSi_2Sb_4 presents dramatically large hole mobility of 1.83×10^5 $cm^2V^{-1}s^{-1}$ along the y-direction with SOC, which is not only beyond those of monolayer α_1-MSi_2Z_4 but also close to that of phosphorene and graphene[56-57] (see Fig. 6). Interestingly, it is found that all of the hole mobilities are significantly higher than the electron's mobilities (see Table 2). There are two aspects reasons. On the one hand, the efficient masses of holes are lower than electrons in most cases, which can be confirmed in curvatures between the CBMs and VBMs in band structures. On the other hand, the low distortion potential of holes can also result in higher hole mobilities. Based on the above, the proposed α_2-MSi_2Z_4 monolayers may be more advantageous for optoelectronic devices on account of their extremely higher carrier mobilities.

Table 2 Electrons and Holes' Carrier Mobilities (μ) at 300 K in Single-Layer MSi_2Z_4 (M = Mo/W, Z = P, As, Sb). The GGA-PBE calculation method used in all calculation results is in Table 2. (x = Zigzag, y = Armchair). Y and N are represented with and without SOC effect in monolayer MSi_2Z_4.

Carrier type	Structure	SOC	Effective masse		Deformation Potential (eV)		2D Elastic Modulus ($J\cdot m^{-2}$)		Mobility ($10^4 cm^2V^{-1}s^{-1}$)	
			m_x^*/m_e	m_y^*/m_e	$\lvert E_{lx}\rvert$	$\lvert E_{ly}\rvert$	C_{2Dx}	C_{2Dy}	μ_x	μ_y

e	α_1-$MoSi_2P_4$	N	0.45	0.43	5.50	5.50	270.56	273.61	0.10	0.10
		Y	0.41	0.43	7.72	8.27	215.46	215.43	0.05	0.04
	α_2-$MoSi_2P_4$	N	0.50	0.50	5.00	5.00	277.78	279.31	0.01	0.01
		Y	0.49	0.49	5.00	5.00	277.95	278.64	0.01	0.01
	α_1-$MoSi_2As_4$	N	0.81	0.78	4.30	4.27	222.08	225.03	0.04	0.04
		Y	0.82	0.78	4.24	4.24	221.87	224.82	0.04	0.04
	α_2-$MoSi_2As_4$	N	0.96	0.96	3.88	3.88	233.85	231.54	0.04	0.04
		Y	0.92	0.92	3.82	3.81	218.39	230.72	0.04	0.04
	α_1-$MoSi_2Sb_4$	N	1.64	1.17	2.57	2.61	149.49	168.38	0.02	0.03
		Y	1.67	0.96	2.36	2.54	148.98	167.82	0.03	0.05
	α_2-$MoSi_2Sb_4$	N	1.52	1.48	2.36	2.40	168.64	180.38	0.03	0.03
		Y	1.35	1.39	2.30	2.34	168.13	179.82	0.04	0.04
	α_1-WSi_2P_4	N	0.20	0.21	4.78	4.78	281.68	283.07	0.64	0.61
		Y	0.15	0.15	7.90	8.03	217.50	218.37	0.33	0.32
	α_2-WSi_2P_4	N	0.45	0.43	4.43	4.43	290.15	291.08	0.16	0.16
		Y	0.59	0.59	6.86	6.93	227.49	227.49	0.03	0.03
	α_1-WSi_2As_4	N	0.33	0.33	3.86	3.84	232.20	233.03	0.31	0.31
		Y	0.17	0.17	3.89	3.89	229.16	232.28	1.12	1.13
	α_2-WSi_2As_4	N	1.18	1.01	3.40	3.27	244.37	244.00	0.04	0.04
		Y	0.44	0.37	3.43	3.39	242.94	235.04	0.25	0.29
	α_1-WSi_2Sb_4	N	0.52	0.49	2.54	2.54	138.79	158.83	0.18	0.21
		Y	0.16	1.07	1.85	1.81	148.33	164.57	0.07	0.09
	α_2-WSi_2Sb_4	N	1.27	1.50	1.71	1.76	175.22	180.69	0.07	0.06
		Y	0.20	0.19	1.70	1.60	179.10	174.69	3.39	3.93
h	α_1-$MoSi_2P_4$	N	0.39	0.39	3.53	3.53	270.56	273.61	0.31	0.31
		Y	0.37	0.38	4.60	5.01	215.46	215.43	0.16	0.13
	α_2-$MoSi_2P_4$	N	0.52	0.52	2.23	2.23	277.78	279.31	0.44	0.44
		Y	0.59	0.58	2.16	2.16	277.95	278.64	0.37	0.38
	α_1-$MoSi_2As_4$	N	0.51	0.49	2.71	2.69	222.08	225.03	0.25	0.27
		Y	0.44	0.42	2.71	2.70	221.87	224.82	0.34	0.36
	α_2-$MoSi_2As_4$	N	0.61	0.61	1.68	1.68	233.85	231.54	0.48	0.47
		Y	0.55	0.55	1.63	1.62	218.39	230.72	0.58	0.62
	α_1-$MoSi_2Sb_4$	N	0.59	0.53	1.92	1.92	149.49	168.38	0.26	0.33
		Y	0.45	0.40	1.94	1.95	148.98	167.82	0.44	0.56
	α_2-$MoSi_2Sb_4$	N	0.68	0.69	1.17	1.15	168.64	180.38	0.56	0.62
		Y	0.58	0.58	1.12	1.10	168.13	179.82	0.85	0.94
	α_1-WSi_2P_4	N	0.26	0.26	3.58	3.56	281.68	283.07	0.69	0.71
		Y	0.11	0.11	5.17	5.27	217.50	218.37	1.44	1.39
	α_2-WSi_2P_4	N	0.39	0.39	1.92	1.92	290.15	291.08	1.10	1.11
		Y	0.27	0.27	2.99	3.04	227.49	227.49	0.75	0.75
	α_1-WSi_2As_4	N	0.33	0.33	2.70	2.70	232.20	233.03	0.62	0.63
		Y	0.13	0.13	2.66	2.67	229.16	232.28	4.09	4.11
	α_2-WSi_2As_4	N	0.44	0.44	1.45	1.46	244.37	244.00	1.28	1.26
		Y	0.28	0.28	1.21	1.21	242.94	235.04	4.52	4.37
	α_1-WSi_2Sb_4	N	0.38	0.35	1.92	1.92	138.79	158.83	0.58	0.73
		Y	0.15	0.14	2.02	1.99	148.33	164.57	3.57	4.37
	α_2-WSi_2Sb_4	N	0.48	0.47	0.96	0.93	175.22	180.69	1.78	2.00
		Y	0.20	0.19	0.76	0.74	179.10	174.69	16.97	18.37

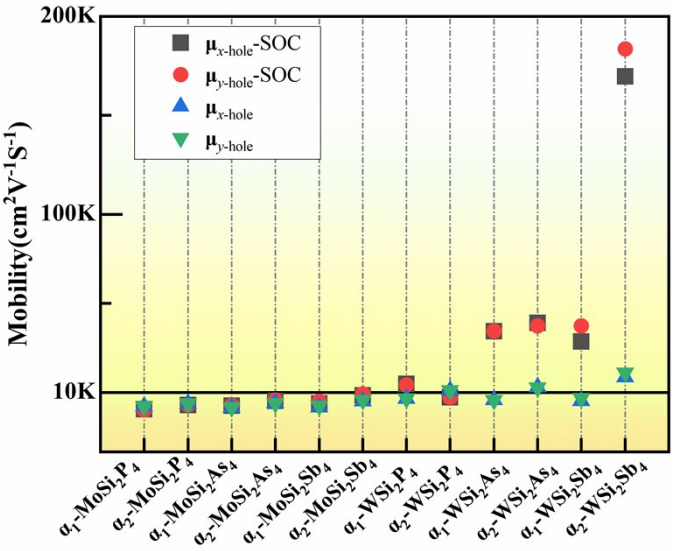

Fig. 6 Calculated hole carrier mobility with/without SOC as shown in Table 2 for monolayer MSi_2Z_4

(M = Mo/W, Z = P, As, Sb).

The direct band gap performance of α_2-$MoSi_2P_4$ calculated by the HSE06 method (with SOC) is 1.07 eV as shown in Fig. S12, manifesting that α_2-$MoSi_2P_4$ monolayer is well suited as donor materials for cell solar.[58] In order to implement the potential applications for solar cells, it is important to look for the proper substrates of single materials. Our calculations using the HSE06 (with SOC) method show that the vacuum-level corrected CBM and VBM for α_2-$MoSi_2P_4$ are located in -4.50 eV and -5.57 eV. After careful investigation of multifarious 2D materials, monolayer SIn_2Te[59] was found to be the outstanding acceptor material for α_2-$MoSi_2P_4$, which has CBM and VBM of -4.58 eV and -6.12 eV, respectively. Apparently, α_2-$MoSi_2P_4$ exhibits type-II heterojunction alignment, as seen in Fig. 7(a). According to the formula listed in the supporting information, the power conversion efficiencies (PCEs) of α_2-$MoSi_2P_4$/SIn_2Te were obtained, as seen in Fig. 7(b). We found that the maximum PCEs of the α_2-$MoSi_2P_4$/SIn_2Te is 20.3%, which is comparable to that of the highly efficient perovskite solar cells.[58]

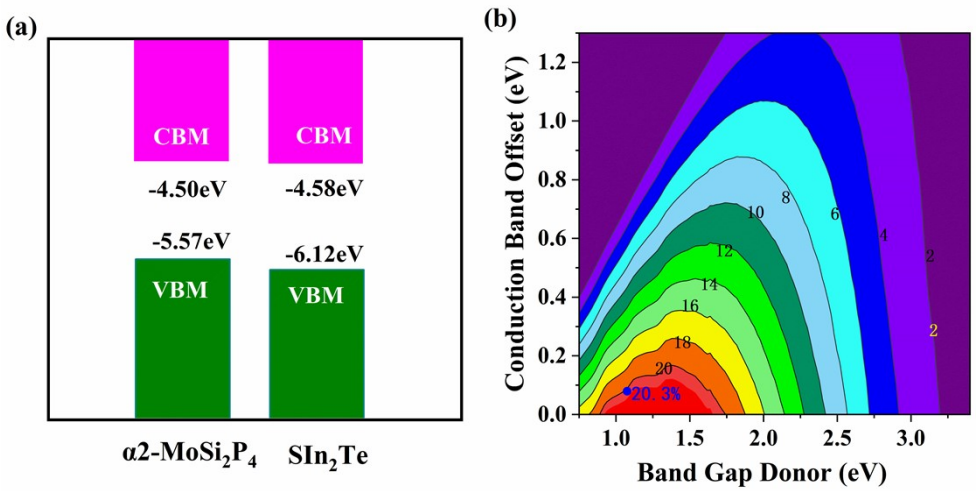

Fig. 7 (a) Schematic diagram of the donor-acceptor band edges of α_2-$MoSi_2P_4$(with SOC) and SIn_2Te monolayers calculated by the HSE06 method. (b) Solar energy transformation efficiency. Yellow and blue dots indicate PCEs for the α_2-$MoSi_2P_4$/SIn_2Te system.

Conclusion

In summary, we proposed two new α_1-phase $MoSi_2Sb_4$ and WSi_2Sb_4 monolayers,

and a family of one-layer α_2-phase MSi_2Z_4 (M = Mo, W; Z = P, As, Sb) proven by the phonon calculations, cohesion energy, and AIMD simulations. Cohesion energy indicates that α_2-phase structures are more stable than α_1-phase structures, possessing high stability in ambient conditions due to the large O_2 decomposition of the barrier. Remarkably, all of these monolayer MSi_2Z_4 are direct band gap semiconductors with fascinating optical absorption ranging from infrared to visible light by HSE06 level. Moreover, most of the electrons and hole mobilities are beyond the 10^3 $cm^2V^{-1}s^{-1}$, the largest is up to 10^5 $cm^2V^{-1}s^{-1}$ for α_2-WSi_2Sb_4. Interestingly, it is found that all of the hole mobilities are significantly higher than the electron's mobilities. The SOC effect significantly reduced the effective mass of carriers, which will result in outstanding carrier mobility. These monolayer MSi_2Z_4 will have potential applications in photoelectric devices due to their larger carrier mobilities. In addition, the monolayer α_2-$MoSi_2P_4$ is anticipated to have a desirable power conversion efficiency of 20.3%, suggesting that α_2-$MoSi_2P_4$ is prospective donor material for solar cells. Our finding shows that these monolayer $MoSi_2N_4$ semiconductors have dramatic potential applications in high-performance optoelectronic devices.

Conflicts of interest

The authors declare no competing financial interest.

Acknowledgments

This work was supported in part by the Natural Science Foundation of China under Grant (No.12174040, 12147102, and 12204398), Chongqing Natural Science Foundation under Grant (No. cstc2020jcyj-msxmX0118). Education Department of Hunan Province (21C0093) and the Foshan (Southern China) Institute for New Materials (2021A1515110127).

References

1 C. Lan, Z. Zhou, R. Wei and J.C. Ho, *Mater. Today Energy*, 2019, **11**, 61-82.

2 X. Wang, J. He, B. Zhou, Y. Zhang, J. Wu, R. Hu, L. Liu, J. Song and J. Qu, Song, J. and Qu, J., *Angew. Chem. Int. Ed.*, 2018, **130**, 8804-8809.

3 J. Dai and X. C. Zeng, *J. Phys. Chem. Lett.*, 2014, **5**, 1289-1293.
4 W. Xu, Y. Jin, B. Zheng and H. Xu, *J. Phys. Chem. C.*, 2018, **122**, 27590-27596.
5 S. Manzeli, D. Ovchinnikov, D. Pasquier, O.V. Yazyev and A. Kis, 2017, **2**, 1-15.
6 S. Manzeli, D. Ovchinnikov, D. Pasquier, O.V. Yazyev, A. Kis and Wang, X., *Adv. Funct.Mater.*, 2017, **27**, 1604093.
7 B. Radisavljevic, A. Radenovic, J. Brivio, V. Giacometti and A. Kis, *Nat. Nanotechnol.*,2011, **6**, 147-150.
8 H. Shi, S. Fu, Y. Liu, C. Neumann, M. Wang, H. Dong, P. Kot, M. Bonn, H.I. Wang and A. Turchanin, *Adv. Mater.*, 2021, **33**, 2105694.
9 J. Qiao, X. Kong, Z.-X. Hu, F. Yang and W. Ji, *Nat.*, *Commun.* 2014, **5**, 1-7.
10 F. Xia, H. Wang and Y. Jia, *Nat. Commun.*, 2014, **5**, 1-6.
11 S.P. Koenig, R.A. Doganov, H. Schmidt, A. Castro Neto and B. Özyilmaz, *Appl. Phys. Lett.*, 2014, **104**, 103106.
12 A. Castellanos-Gomez, L. Vicarelli, E. Prada, J.O. Island, K. Narasimha-Acharya, S.I. Blanter, D.J. Groenendijk, M. Buscema, G.A. Steele and J. Alvarez, *2D Mater.*, 2014, **1**, 025001.
13 X. Ling, H. Wang, S. Huang, F. Xia and M.S. Dresselhaus, *Proc. Natl. Acad. Sci. U.S.A.*, 2015, **112**, 4523-4530.
14 S C. Sun, H. Xiang, B. Xu, Y. Xia, J. Yin and Z.J.A.P.E. Liu, *Appl. Phys. Express*, 2016, **9**, 035203.
15 M. Obeid, A. Bafekry, S.U. Rehman and C.V. Nguyen, *Appl. Surf. Sci.*, 2020, **534**, 147607.
16 B. Marfoua and J. Hong, *Nanotechnology*, 2020, **32**, 115702.
17 R. Meng, X. Sun, D. Yang, J. Bao and X. Chen, *Appl. Mater.*, 2018, **13**, 276-284.
18 J Y. Jing, Y. Ma, Y. Li and T. Heine, *Nano Lett.*, 2017, **17,** 1833-1838.
19 L.-P. Feng, A. Li, P.-C. Wang and Z.-T. Liu, *J. Phys. Chem. C.*, 2018, **122**, 24359-24367.
20 Z. Sun, K. Yuan, Z. Chang, S. Bi, X. Zhang and D. Tang, *Nanoscale*, 2020, **12**, 3330-3342.
21 A.D. Oyedele, S. Yang, L. Liang, A.A. Puretzky, K. Wang, J. Zhang, P. Yu, P.R. Pudasaini, A.W. Ghosh and Z. Liu, *J. Am. Chem. Soc.*, 2017, **139**, 14090-14097.
22 F. Li, X. Liu, Y. Wang and Y.J.J.o.M.C.C. Li, *J. Mater. Mater. C.*, 2016, **4**, 2155-2159.
23 L.-B. Shi, M. Yang, S. Cao, Q. You, Y.-Y. Niu and Y.-Z., *Appl. Surf. Sci.*, 2019, **492**, 435-448.
24 P. Zhao, J. Li, W. Wei, Q. Sun, H. Jin, B. Huang and Y. Dai, *Phys. Chem. Chem. Phys.*, 2017, **19**, 27233-27239.
25 S. Guo, Y. Zhang, Y. Ge, S. Zhang, H. Zeng and H. Zhang, *Adv. Mater.*, 2019, **31**, 1902352.
26 H. Shu, *Mater. Res. Express*, 2018, **6**, 026428.
27 Z. Shu, Q. Peng, P. Huang, Z. Xu, A.A. Suleiman, X. Zhang, X. Bai, X. Zhou and T. Zhai, *Matter*, 2020, **2**, 977-987.
28 W. Xu, Z. Xie, J. Su, R. Wang, X. Wu and H. Xu, *J. Phys. Chem. Lett.*, 2021, **12**, 10574-10580.
29 Y. Jing, Z. Zhou, J. Zhang, C. Huang, Y. Li, and F. Wang, *Phys. Chem. Chem. Phys.*, 2019, **21**, 21064-21069.
30 Y. Jing, Z. Zhou, J. Zhang, C. Huang, Y. Li, F. Wang and F. Wang, *Phys. Chem. Chem. Phys.*, 2019, **21,** 21064-21069.
31 Y.-L. Hong, Z. Liu, L. Wang, T. Zhou, W. Ma, C. Xu, S. Feng, L. Chen, M.-L. Chen and D.-M. Sun, *Science*, 2020, **369**, 670-674.
32 B. Mortazavi, B. Javvaji, F. Shojaei, T. Rabczuk, A.V. Shapeev and X. Zhuang, *Nano Energy*, 2021, **82**, 105716.

33 L. Wang, Y. Shi, M. Liu, A. Zhang, Y.-L. Hong, R. Li, Q. Gao, M. Chen, W. Ren and H.-M. Cheng, *Nat. Commun.*, 2021, **12**, 1-10.
34 J.-S. Yang, L. Zhao, L. Shi-Qi, H. Liu, L. Wang, M. Chen, J. Gao and J. Zhao, *Nanoscale*, 2021, **13**, 5479-5488.
35 J. Hafner, *J. Comput. Chem.*, 2008, **29**, 2044-2078.
36 J. Hafner, *Comput. Phys. Commun.*, 2007, **177**, 6-13.
37 G. Sun, J. Kürti, P. Rajczy, M. Kertesz, J. Hafner and G. Kresse, *J. Mol. Struct. Theochem.*, 2003, **624**, 37-45.
38 J. Perdew, K. Burke and M. Ernzerhof, *Phys. Rev. Lett.*, 1998, **80**, 891.
39 M. Ernzerhof and G.E. Scuseria, *J. Chem. Phys.*, 1999, **110**, 5029-5036.
40 C. Adamo and V. Barone, *J. Chem. Phys.*, 2002, **116**, 5933-5940.
41 A.D. Boese and N.C. Handy, *J. Chem. Phys.*, 2001, **114**, 5497-5503.
42 A.V. Krukau, O.A. Vydrov, A.F. Izmaylov and G.E. Scuseria, *J. Chem. Phys.*, 2006, **125**, 224106.
43 D. Le, A. Kara, E. Schröder, P. Hyldgaard and T.S. Rahman, *J. Phys. Condens. Matter.*, 2012, **24**, 424210.
44 G. Henkelman, B.P. Uberuaga and H. Jónsson, *J. Chem. Phys.*, 2000, **113**, 9901-9904.
45 H. Yao, C. Zhang, Q. Wang, J. Li, Y. Yu, F. Xu, B. Wang and Y. Wei, *Nanomaterials*, 2021, **11**, 559.
46 S. Ahmad and S. Mukherjee, *Graphene*, 2014, **03**, 52-59.
47 J. Guan, Z. Zhu and D. Tománek, *Phys. Rev. Lett.*, 2014, **113**, 046804.
48 G. Pastore, E. Smargiassi and F. Buda, *Phys. Rev. A*, 1991, **44**, 6334.
49 G. Wang, R. Pandey and S.P. Karna, *WIREs. Comput. Mol. Sci.*, 2017, **7**, 3537717.
50 J.L. Zhang, C. Han, Z. Hu, L. Wang, L. Liu, A.T. Wee and W. Chen, *Adv. Mater.*, 2018, **30**, 1802207.
51 Y.Z. Zhang, Y. Wang, Q. Jiang, J.K. El-Demellawi, H. Kim and H.N. Alshareef, *Adv. Mater.*, 2020, **32**, 1908486.
52 Z. Li, L. Wang, D. Sun, Y. Zhang, B. Liu, Q. Hu, A. Zhou and E. B, *Mater. Sci.*, 2015, **191**, 33-40.
53 A. Ziletti, A. Carvalho, D.K. Campbell, D.F. Coker and A.C. Neto,*Phys. Rev. Lett.*, 2015, **114**, 046801.
54 S. Wan, F. Gándara, A. Asano, H. Furukawa, A. Saeki, S.K. Dey, L. Liao, M.W. Ambrogio, Y.Y. Botros and X. Duan, *Chem. Mater.*, 2011, **23**, 4094-4097.
55 J. Bardeen and W.S. Shockley, *Phys. Rev.*, 1950, **80**, 72-80.
56 K.I. Bolotina, K.J. Sikes, Z. Jiang , M. Klimac , G. Fudenberg , J. Hone , P. Kim and H.L. Stormer. *Solid State Commun*. 2008, **146**, 351-355.
57 A. Carvalho, M. Wang, X. Zhu, A.S. Rodin, H. Su and A.H. Castro Neto, *Nat. Rev. Mater.*, 2016, **1**, 1-16.
58 W. Hu, L. Lin, C. Yang, J. Dai and J. Yang, *Nano letters*, 2016, **16**, 1675-1682.
59 X. Li, B. Zhai, X. Song, Y. Yan, J. Li and C. Xia, *Appl. Surf. Sci.*, 2020, **509**, 145317.